Electronic Supplementary Information (ESI)

Long-chain tin(IV) alkanethiolates ($Sn(SC_nH_{2n+1})_4$, n≥12) with the coexistence of *trans* and *gauche* S−C bonds: a class of lamellar van der Waals molecular crystals

Tingting Wang, Yixin Wan, Nan Yu, Kewei Gu, Zhiwei Lu, and Junli Wang*

School of Materials Science & Engineering, Jiangsu University, Zhenjiang 212013, PR China.

E-mail: wangjl@ujs.edu.cn

1. Experimental section

1.1 Synthesis of polycrystalline solids

All chemicals were purchased from Aladdin Biochemical Technology Co., Ltd.: tin chloride pentahydrate ($SnCl_4·5H_2O$, 99.0%, AR), 1-dodecanethiol ($C_{12}H_{25}SH$, 98%), 1-tetradecanethiol ($C_{14}H_{29}SH$, >97%), 1-hexadecanethiol ($C_{16}H_{33}SH$, >97%), 1-octadecanethiol ($C_{18}H_{37}SH$, 97%), and ethanol (>99.5%)

In a typical synthetic procedure of Sn(VI) alkanethiolates ($Sn(SC_nH_{2n+1})_4$), 1 mmol (0.3506 g) $SnCl_4·5H_2O$ was dissolved in 3−5 mL of 1-alkanethiols (HSC_nH_{2n+1}, n=12, 14, 16 and 18) in a three-necked flask. The solution was heated to 120 °C and kept at this temperature for 30 min under magnetic stirring, which generates a colorless solution. When naturally cooled, white polycrystalline powders were obtained after the following processes: precipitated by adding ethanol into the mother solution, further purified by three times of chloroform dissolving, ethanol precipitation and centrifugation, and finally dried in a vacuum oven at room temperature. For the preparation of $Sn(SC_{12}H_{25})_4$, after the addition of ethanol, the solution of $Sn(SC_{12}H_{25})_4$ was allowed to stand overnight (at room temperature or better in a 4 °C refrigerator) in order to flocculate its polycrystalline precipitate. The as-obtained Sn(VI) alkanethiolates could be well dissolved in chloroform or toluene and then precipitated again by adding ethanol.

We note that Stam and colleagues [1] reported the presence of $Sn(SC_{12}H_{25})_4$ Sn(IV)−thiolate complex at the surface of $Cu_{2-x}S$ colloidal nanocrystals by means of solid-state ^{119}Sn NMR and that they used a synthetic protocol that adds CuCl and $SnBr_4$ into a mixture of 1-dodecanethiol ($HSC_{12}H_{25}$) and oleylamine to react at 225 °C. In this work, pure $Sn(SC_{12}H_{25})_4$ was not isolated. Oleylamine may pollute Sn(IV)−thiolate complexes. Therefore, our synthesis of Sn(VI) alkanethiolates ($Sn(SC_nH_{2n+1})_4$), n=12, 14, 16 and 18) was performed in pure 1-alkanethiols. This synthetic method has been recently employed for preparing Bi(III) dodecanethiolate

($Bi(SC_{12}H_{25})_3$, see Ref. 10).

[1**]** W. van der Stam, S. Gradmann, T. Altantzis, X. Ke, M. Baldus, S. Bals and C. de M. Donega, *Chem. Mater.*, 2016, **28**, 6705−6715.

1.2 Growth of single crystals

Growth of single crystals could be performed using two methods. One was the liquid-liquid diffusion method. An appropriate amount of Sn(VI) alkanethiolates was dissolved in 2 mL $CHCl_3$ and then transferred to a glass tube (diameter × length: 0.5 × 18 cm). Afterwards, 1 mL of $CHCl_3$/EtOH (v:v=1:2) mixed solution was added as a transition layer and the rest of the tube was filled with EtOH. The culture tube was finally sealed with the parafilm (PM992) and placed in a dark, quiet environment. One or two holes could be made with a thin needle at the sealing parafilm in order to promote the evaporation of solvents and the diffusion of molecules. The colorless, transparent, flake-like crystals were obtained within 1 to 2 weeks (Fig. S7).

The other one was the solvent evaporation method. In brief, an appropriate amount of $Sn(SC_nH_{2n+1})_4$ polycrystalline powders was dissolved in 2 mL $CHCl_3$/EtOH (v:v=5:1−3:1) in a small sample bottle. This bottle was then placed in a larger glass bottle that contained 2−4 mL $CHCl_3$/EtOH with a low v:v ratio (1:1). After the larger bottle was sealed, $CHCl_3$ would slowly evaporate to form supersaturated solution in the small bottle for growing single crystals. The bottles were placed in a dark, quiet environment. The colorless, transparent, flake-like crystals were obtained within 1 to 2 weeks. The volume capacities for the small and large bottles were 4 and 20 mL.

1.3 Characterizations

Powder XRD

The powder XRD patterns of $Sn(SC_nH_{2n+1})_4$ polycrystalline samples were collected in the range of 2−60° (2θ) on a Rigaku Ultimate IV X-ray diffractometer (Cu Ka radiation λ=1 .5418 Å) operated at 40 KV and 40 mA. The powder XRD data of the SnS products were collected on a D8 Advance diffractometer with graphite-monochromatized Cu Kα radiation (λ=1.54178 Å, Bruker-AXS). All of the XRD data were collected at room temperature.

Single crystal XRD

The single crystal data of $Sn(SC_{12}H_{25})_4$ and $Sn(SC_{14}H_{29})_4$ were collected at low temperature using a Bruker APEX-II CCD diffractometer with Cu Kα radiation (λ = 1.54184 Å). The single crystal data of $Sn(SC_{16}H_{33})_4$ were collected at room temperature on a Bruker D8 Venture X-ray diffractometer with graphite monochromated Mo Kα radiation (λ = 0.71073 Å). Using Olex2 [1], the structures for three crystals were solved with the SHELXT [2] structure solution program using Intrinsic Phasing and refined with the SHELXL [3] refinement package using Least Squares minimization.

[1] Dolomanov, O.V., Bourhis, L.J., Gildea, R.J, Howard, J.A.K. & Puschmann, H. (2009), J. Appl. Cryst. 42, 339-341.
[2] Sheldrick, G.M. (2008). Acta Cryst. A64, 112-122.
[3] Sheldrick, G.M. (2015). Acta Cryst. C71, 3-8.

FT-IR

Fourier transform infrared spectra (FT-IR) recorded on a Nicolet FT-170SX Fourier transform spectrometer using an attenuated total reflection (ATR) model within the wavenumber range of 400–4000 cm^{-1}.

TG-DSC

A NETZSCH STA 449 F3 thermal analyzer was used to collect the thermogravimetry and differential scanning calorimetry (TG-DSC) data for the thermolysis of Sn(VI) alkanethiolates. The sample purge N_2 flow was 60 mL/min and the flow of N_2 protection was 20 mL. The heating rate was 10 °C/min.

DSC

The DSC heating/cooling cycles of $Sn(SC_nH_{2n+1})_4$ samples were recorded on SDT Q600 thermal analyzer in the temperature range of 0 °C−100 °C−0 °C. The purge N_2 flow was 100 mL/min and the scanning rate was 10 °C/min.

2. Supporting figures

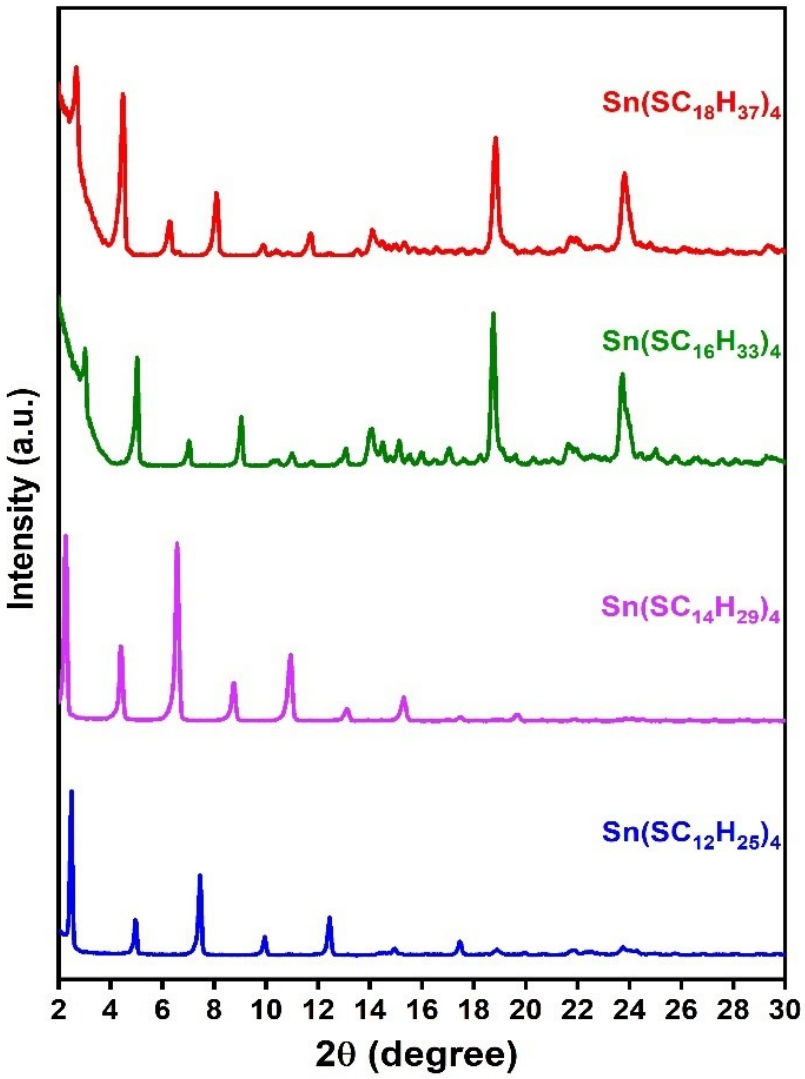

Fig. S1 The p-XRD patterns recorded on $(Sn(SC_nH_{2n+1})_4$ (n=12, 14, 16 and 18) polycrystalline powders. As seen in other metal alkanethiolates (see refs. 3−11 and 14), a series of successive (h00) diffraction peaks with an equal spacing distance at the low 2θ-angle region are present, suggesting a layered crystal structure for $(Sn(SC_nH_{2n+1})_4$ homologous crystals. It can be observed that the XRD profile of $Sn(SC_{12}H_{25})_4$ is very similar to that of $Sn(SC_{14}H_{29})_4$ while the XRD profile of $Sn(SC_{16}H_{33})_4$ is very similar to that of $Sn(SC_{18}H_{37})_4$. A collective shift of diffraction lines to the small 2θ-angle positions occurs with the increase in the chain lengths of alkyl chains in $Sn(SC_nH_{2n+1})_4$.

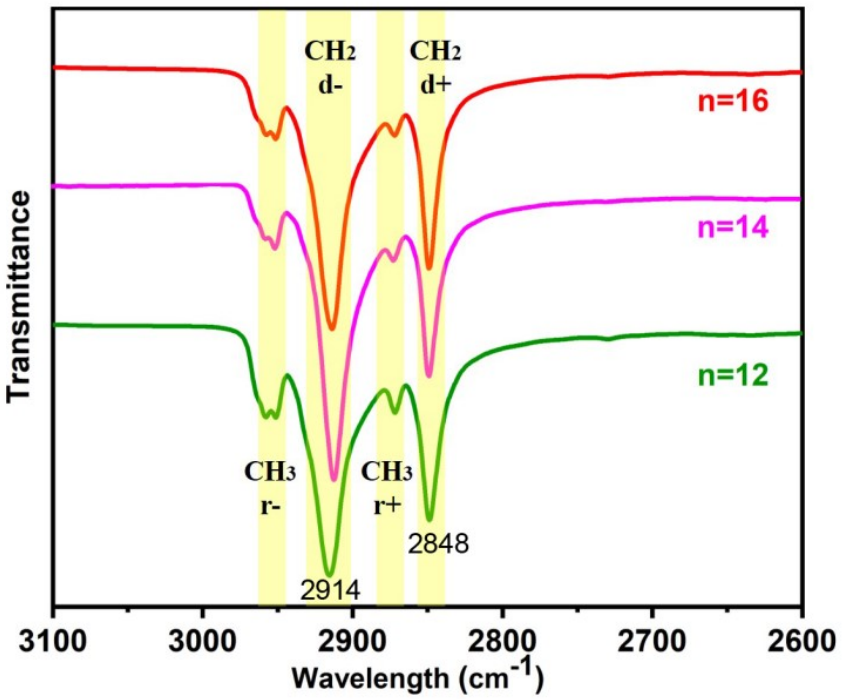

Fig. S2 FTIR spectra recorded on ($Sn(SC_nH_{2n+1})_4$ (n = 12, 14 and 16) polycrystalline powders. The presence of the strong symmetric (d+) and antisymmetric (d-) CH_2 stretching bands with peak maxima around 2848 and 2914 cm^{-1} indicates that long C_nH_{2n+1} chains have a fully extended, all-*trans* conformation (see refs. 4−6).

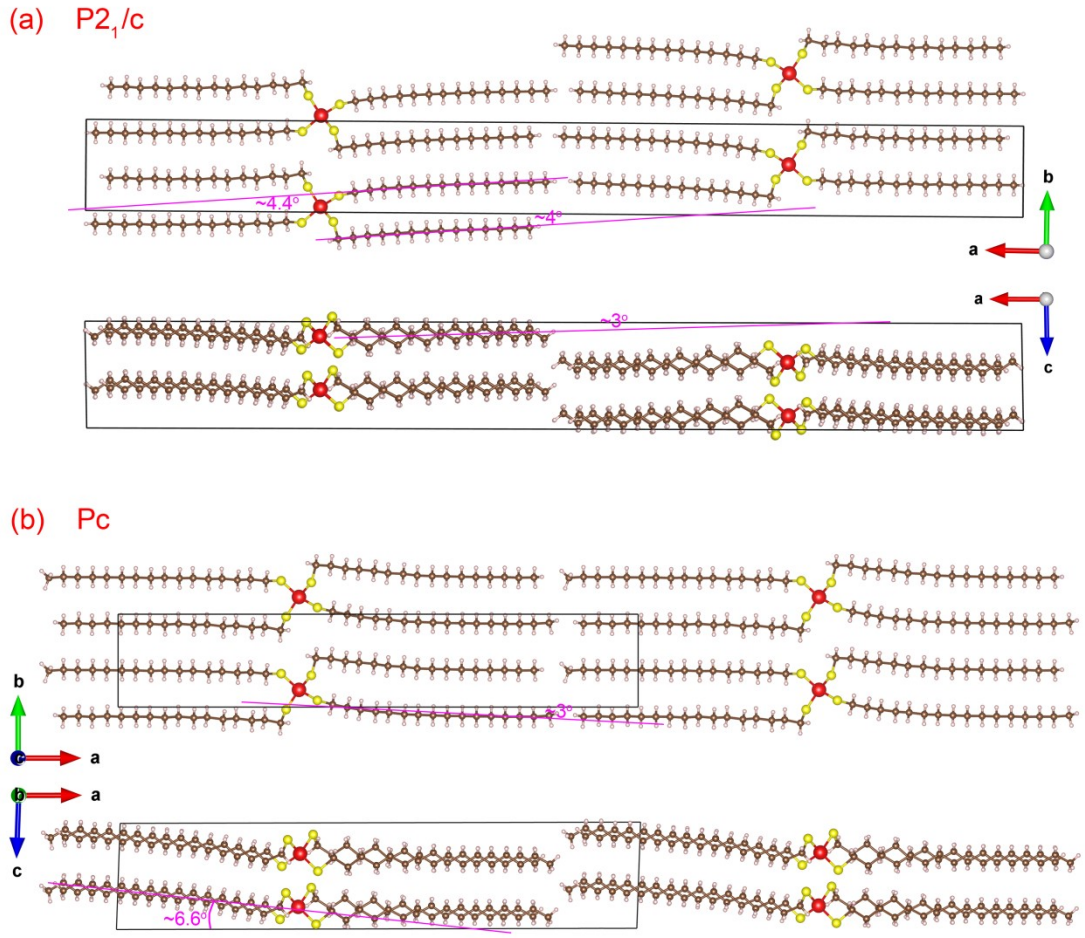

Fig. S3 Schematic illustration for measuring the tilt angles of C_nH_{2n+1} chains relative to ***a*** axis. All C_nH_{2n+1} chains extend along ***a*** axis and their chain axes prefer to be parallel to ***a*** axis as possible as they can. In both unit cells, the maximum value for the tilt angles is below 7°. In the top figure of (a) and (b), the lower sublayer of $Sn(SC_nH_{2n+1})_4$ molecules is omitted for a better observation.

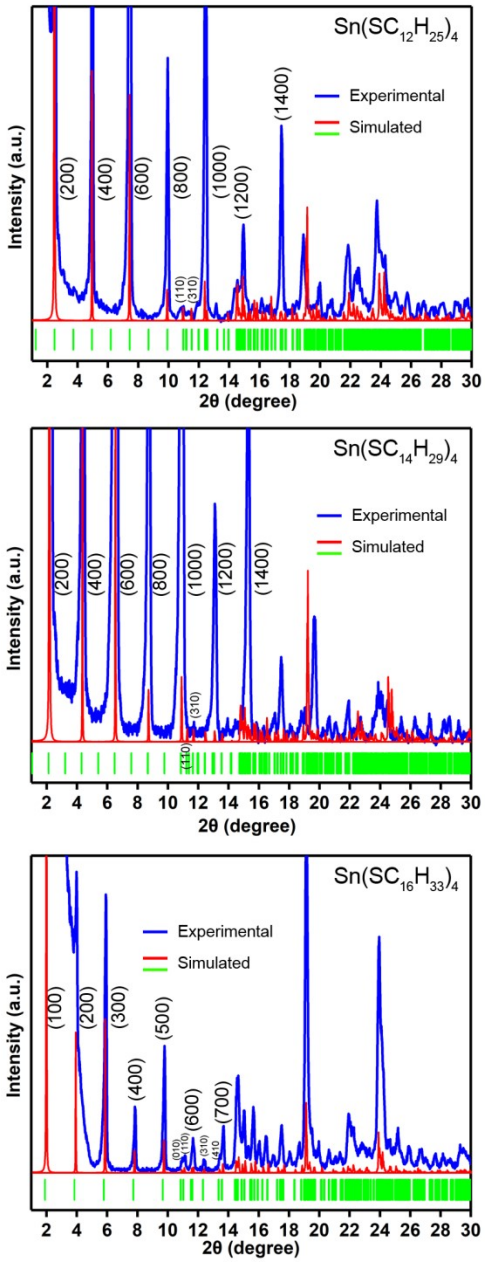

No.	h	k	l	d (Å)	F(real)	F(imag)	|F|	2θ	I
1	1	0	0	71.38929	-1.65602	-0.0736221	1.65766	1.23648	0.0084
2	2	0	0	35.69465	-359.567	-30.2557	360.838	2.4731	100.0000
3	3	0	0	23.79643	-2.03277	0.209293	2.04351	3.71001	0.0014
4	4	0	0	17.84732	205.449	29.2647	207.523	4.94735	8.2516
5	5	0	0	14.27786	-5.97878	-0.348379	5.98892	6.18527	0.0044
6	6	0	0	11.89822	-316.415	-28.1852	317.668	7.42391	8.5636
7	7	0	0	10.19847	2.6046	0.458331	2.64462	8.66342	0.0004
8	8	0	0	8.92366	165.732	26.3626	167.816	9.90395	1.3378
9	1	1	0	8.06798	85.1119	9.34713	85.6236	10.9574	0.5679
10	9	0	0	7.93214	-3.64303	-0.555285	3.68511	11.1456	0.0005
11	2	1	0	7.91772	-10.1393	-0.33474	10.1448	11.166	0.0077
12	3	1	0	7.68491	-88.0226	-9.26434	88.5088	11.5054	0.5498
13	4	1	0	7.39099	-14.2918	0.567871	14.3031	11.9646	0.0133
14	10	0	0	7.13893	-244.262	-24.605	245.498	12.3886	1.8208
15	5	1	0	7.05838	86.5088	9.09712	86.9858	12.5306	0.4468
16	6	1	0	6.70698	-13.1512	-0.783646	13.1746	13.19	0.0092
17	11	0	0	6.48994	1.99437	0.627765	2.09084	13.6331	0.0001
18	7	1	0	6.35242	-88.0972	-8.86428	88.542	13.9297	0.3734
19	0	1	1	6.11500	-100.92	-12.0536	101.637	14.4734	0.4551
20	1	1	-1	6.10092	162.295	18.4933	163.345	14.5069	1.1699
21	1	1	1	6.08450	-162.468	-18.0544	163.468	14.5463	1.1652
22	2	1	-1	6.04315	115.238	12.2399	115.886	14.6464	0.5775
23	2	1	1	6.01136	78.7188	11.8466	79.6052	14.7242	0.2696
24	8	1	0	6.00577	-40.7947	0.743131	40.8014	14.738	0.0707

No.	h	k	l	d (Å)	F(real)	F(imag)	|F|	2θ	I
1	1	0	0	81.16857	-1.35137	-0.0716646	1.35327	1.0875	0.0057
2	2	0	0	40.58429	-358.509	-30.3105	359.788	2.1751	100.0000
3	3	0	0	27.05619	1.81944	0.209413	1.83145	3.26289	0.0012
4	4	0	0	20.29214	212.039	29.489	214.08	4.35098	8.8368
5	5	0	0	16.23371	-4.8438	-0.341306	4.85581	5.43946	0.0029
6	6	0	0	13.52810	-321.597	-28.6523	322.871	6.52843	8.9093
7	7	0	0	11.59551	4.9639	0.455919	4.98479	7.61799	0.0016
8	8	0	0	10.14607	176.369	27.1319	178.444	8.70825	1.5250
9	9	0	0	9.01873	-7.24347	-0.555908	7.26477	9.79929	0.0020
10	10	0	0	8.11686	-263.631	-25.6905	264.879	10.8912	2.1401
11	1	1	0	7.85082	86.8186	9.10731	87.295	11.2615	0.4345
12	2	1	0	7.74291	-3.69207	-0.286071	3.70314	11.4189	0.0008
13	3	1	0	7.57256	-87.969	-9.04263	88.4326	11.6767	0.4144
14	11	0	0	7.37896	6.39968	0.631945	6.43081	11.9842	0.0010
15	4	1	0	7.35191	-14.6911	0.504104	14.6997	12.0284	0.0108
16	5	1	0	7.09465	86.2375	8.91228	86.6968	12.4663	0.3489
17	6	1	0	6.81410	-8.8891	-0.722209	8.91839	12.9817	0.0034
18	12	0	0	6.76405	130.341	23.7555	132.488	13.0782	0.3696
19	7	1	0	6.52188	-85.1317	-8.72675	85.5778	13.566	0.2863
20	13	0	0	6.24374	-7.50835	-0.69101	7.54008	14.1734	0.0010
21	8	1	0	6.22732	-33.7624	0.746509	33.7706	14.211	0.0406
22	0	1	1	6.00226	127.496	14.019	128.264	14.7467	0.5427
23	1	1	-1	5.99149	-139.396	-16.7527	140.399	14.7734	0.6479
24	1	1	1	5.98035	151.086	16.4049	151.974	14.801	0.7563

No.	h	k	l	d (Å)	F(real)	F(imag)	|F|	2θ	I
1	-1	0	0	45.61307	-93.8964	-160.974	186.357	1.93527	100.0000
2	1	0	0	45.61307	-118.709	143.451	186.199	1.93527	99.8302
3	-2	0	0	22.80654	-47.7724	94.4956	105.885	3.87109	8.0604
4	2	0	0	22.80654	-19.7926	-104.419	106.279	3.87109	8.1205
5	3	0	0	15.20436	160.067	62.5425	171.851	5.80802	9.4164
6	-3	0	0	15.20436	167.945	-34.5188	171.456	5.80802	9.3731
7	-4	0	0	11.40327	-62.0155	-66.9492	91.2586	7.74662	1.4892
8	4	0	0	11.40327	-79.5849	45.3161	91.5622	7.74662	1.4998
9	-5	0	0	9.12261	-26.0301	143.161	145.509	9.68743	2.4137
10	5	0	0	9.12261	0.693495	-144.978	144.979	9.68743	2.3962
11	0	1	0	8.13350	50.4216	5.00491	50.6694	10.8689	0.4640
12	-1	1	0	8.00720	-23.9459	-40.6237	47.156	11.0408	0.3894
13	1	1	0	8.00720	-31.9642	34.6932	47.1734	11.0408	0.3897
14	-2	1	0	7.66090	-26.5646	42.4464	50.0737	11.5416	0.4014
15	2	1	0	7.66090	-17.1184	-45.3847	48.5057	11.5416	0.3766
16	-6	0	0	7.60218	66.4852	-29.3653	72.6815	11.631	0.4163
17	6	0	0	7.60218	53.3887	50.8666	73.7412	11.631	0.4285
18	-3	1	0	7.17181	45.897	-11.0849	47.2167	12.3316	0.3121
19	3	1	0	7.17181	42.7165	20.3033	47.2962	12.3316	0.3132
20	-4	1	0	6.62171	-23.7404	-44.9706	50.8524	13.3606	0.3077
21	4	1	0	6.62171	-29.2854	37.1872	47.3342	13.3606	0.2666
22	7	0	0	6.51615	-107.92	34.4878	113.296	13.578	0.7390
23	-7	0	0	6.51615	-98.4446	-56.2969	113.405	13.578	0.7404
24	0	1	1	6.12542	95.1675	22.78	97.856	14.4486	0.9717

Fig. S4 (Left) The fitting results of the lab-experimental p-XRD patterns recorded on polycrystalline solids with the simulated p-XRD patterns derived from single crystals. (Right) The diffraction lines within 2θ=1−14° of simulated p-XRD patterns are provided for information. The diffraction peaks with too weak intensity (I) are invisible in p-XRD patterns.

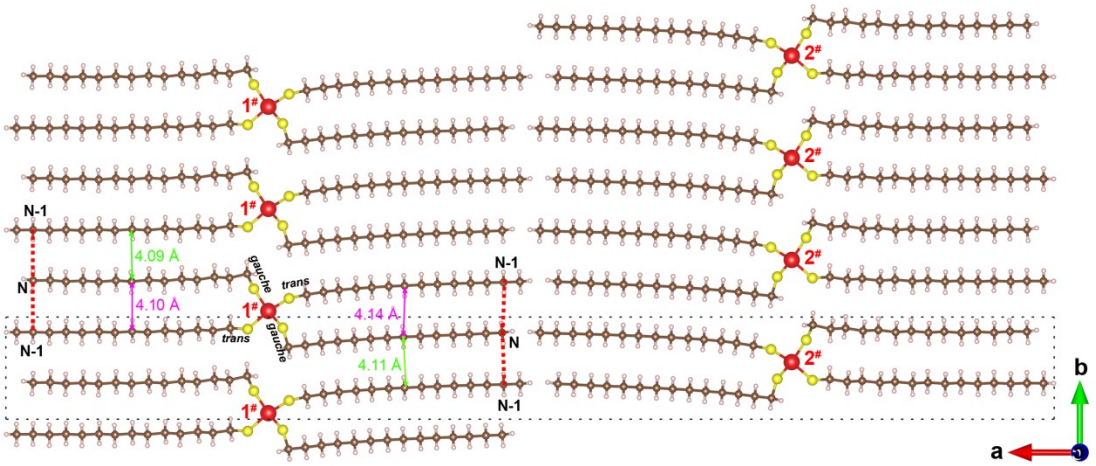

Fig. S5 Schematic illustration for measuring the closest intramolecular and intermolecular chain-chain distances in $Sn(SC_nH_{2n+1})_4$ crystals. It can be observed that the *trans* S-bonded C_nH_{2n+1} chain bulges out by one nonbonded C···C distance along the ***a*** axis direction relative to the *gauche* S-bonded C_nH_{2n+1} chain. The average value for interchain C···C spacings, *which are measured between the Nth C atom in gauche S-bonded C_nH_{2n+1} chain and the (N-1)th C atom in trans S-bonded C_nH_{2n+1} chain (N=2 to n, red dotted lines)*, is used to assess the linear distance (marked with double-headed arrows) between two intramolecular (or intermolecular) neighboring alkyl chains. Taking n=14 as an example, N ranges from 2 to 14, and then the intramolecular *vs* intermolecular chain-chain distances are calculated as follows: 4.12 vs 4.10 Å. This method is also applicable to n=12 and 16.

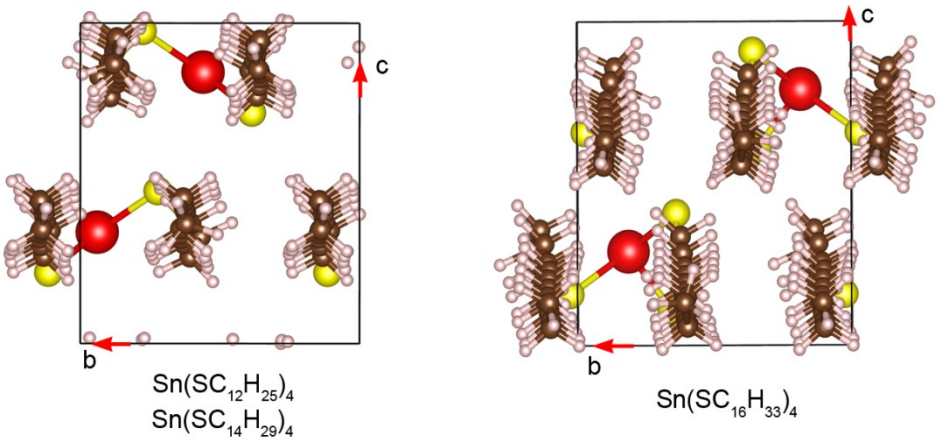

Fig. S6 Unit cells of $Sn(SC_nH_{2n+1})_4$ crystals projected from ***a*** axis, where there are four C_nH_{2n+1} chains extending within the *bc* plane. Other alkyl chains and Sn/S atoms are omitted for a better observation.

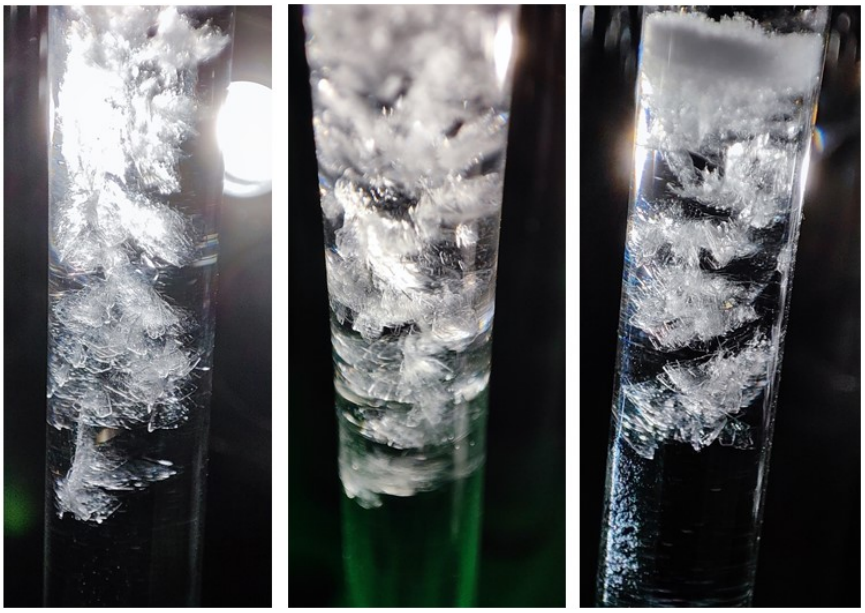

Fig. S7 Optical graphics of $Sn(SC_nH_{2n+1})_4$ single crystals grown by a layering diffusion method in $CHCl_3$/EtOH. From left to right are $Sn(SC_{12}H_{25})_4$, $Sn(SC_{14}H_{29})_4$ and $Sn(SC_{16}H_{33})_4$.

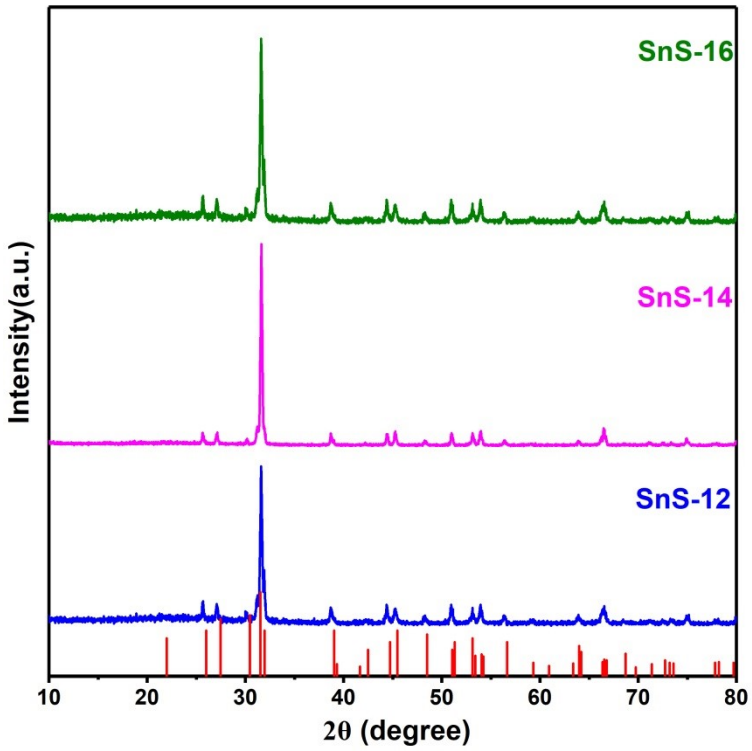

Fig. S8 p-XRD patterns recorded on the solid products obtained from $Sn(SC_nH_{2n+1})_4$ thermal decomposition, all of which are in good agreement with the standard diffraction lines for SnS (shown in red at the bottom, PDF# 73-1859).

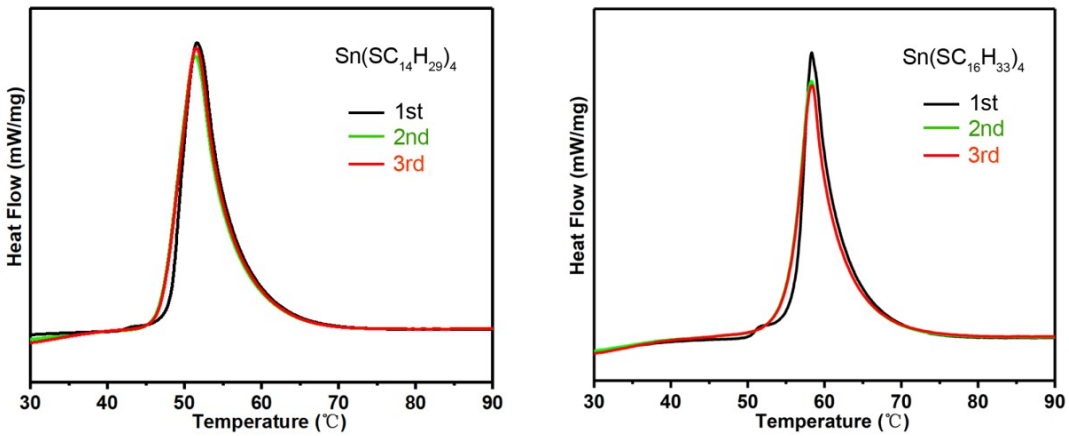

Fig. S9 Multiple DSC melting point measurements for $Sn(SC_nH_{2n+1})_4$. Almost the same melting temperatures are confirmed for each crystal.

3. Supporting tables

Table S1 Sn−S and S−C bond lengths (Å) and ∠S−Sn−S angles (°) in $Sn(SC_nH_{2n+1})_4$ (n=12, 14 and 16) crystals.

Bond lengths	**$Sn(SC_{12}H_{25})_4$**	**$Sn(SC_{14}H_{29})_4$**	**$Sn(SC_{16}H_{33})_4$**
Sn−S(1)	2.432(8)	2.3857(9)	2.376(3)
Sn−S(2)	2.417(9)	2.4056(9)	2.402(3)
Sn−S(3)	2.425(9)	2.3955(9)	2.381(3)
Sn−S(4)	2.413(9)	2.3891(10)	2.407(3)
S(1)−C	1.86(2)	1.836(4)	1.849(13)
S(2)−C	1.86(2)	1.835(4)	1.849(16)
S(3)−C	1.87(2)	1.832(4)	1.808(17)
S(4)−C	1.86(2)	1.833(4)	1.843(10)
Angles			
S(1)-Sn-S(2)	108.0(3)	110.18(3)	110.37(11)
S(1)-Sn-S(3)	110.3(3)	110.12(3)	110.54(11)
S(1)-Sn-S(4)	113.2(3)	104.51(3)	111.76(11)
S(2)-Sn-S(3)	104.9(3)	112.98(3)	103.81(11)
S(2)-Sn-S(4)	110.5(3)	108.83(4)	109.03(12)
S(3)-Sn-S(4)	109.5(4)	109.88(3)	111.03(11)

Notes:

$Sn(SC_{12}H_{25})_4$ and $Sn(SC_{16}H_{33})_4$: S(1) and S(4) in *trans* conformation; S(2) and S(3) in *gauche* conformation.

$Sn(SC_{14}H_{29})_4$: S(2) and S(3) in *trans* conformation; S(1) and S(4) in *gauche* conformation.

Table S2 Crystallographic data for $Sn(SC_nH_{2n+1})_4$ (n=12, 14 and 16) crystals.

Chemical formula	*$Sn(SC_{12}H_{25})_4$	$Sn(SC_{14}H_{29})_4$	$Sn(SC_{16}H_{33})_4$
Formula weight	924.20	1036.41	1148.62
Temperature/K	160.00	150.00	100.00
Crystal system	monoclinic	monoclinic	monoclinic
Space group	$P2_1/c$	$P2_1/c$	Pc
a/Å	71.41(10)	81.184(4)	45.6447(14)
b/Å	8.120(11)	7.8878(4)	8.1335(3)
c/Å	9.297(14)	9.2530(5)	9.3171(3)
α/°	90	90	90
β/°	91.38(4)	91.1170(10)	92.133(3)
γ/°	90	90	90
Volume/Å^3	5389(13)	5924.2(5)	3456.6(2)
Z	4	4	2
ρ_{calc}/g/cm^3	1.139	1.162	1.104
μ/mm^{-1}	5.408	4.969	0.524
F(000)	2008.0	2264.0	1260.0
Radiation	Cu Kα (λ=1.54178)	Cu Kα (λ=1.54178)	Mo Kα (λ=0.71073)
2θ range for data collection	3.712 to 133.152	3.266 to 149.35	4.374 to 59.506
Index ranges	$-84 \le h \le 82$ $-8 \le k \le 8$ $-4 \le l \le 11$	$-99 \le h \le 101$ $-9 \le k \le 9$ $-11 \le l \le 11$	$-57 \le h \le 63$ $-11 \le k \le 11$ $-13 \le l \le 12$
Reflections collected	8786	46808	60728
Independent reflections	6720 R_{int}= 0.0615 R_{sigma}= 0.0963	12081 R_{int}=0.0320 R_{sigma}=0.0338	17139 R_{int} = 0.0798 R_{sigma} = 0.0669
Data/restraints/parameters	6720/368/482	12081/0/554	17139/110/630
Goodness-of-fit on F^2	1.156	1.187	1.112
Final R indexes [I>=2σ (I)]	R_1 = 0.2477 wR_2 = 0.5687	R_1 = 0.0620 wR_2 = 0.1648	R_1 = 0.0809 wR_2 = 0.2176
Final R indexes [all data]	R_1 = 0.2569 wR_2 = 0.5722	R_1 = 0.0639 wR_2 = 0.1672	R_1 = 0.0846 wR_2 = 0.2241
Largest diff. peak/hole / e Å^{-3}	2.18/-5.34	1.47/-0.85	1.22/-0.91

***The reasons for large R_1 and wR_2 values for $Sn(SC_{12}H_{25})_4$ are as follows: 1) the quality of single crystal is not good enough, 2) the data is not completely collected. Although we have tried our best to grow $Sn(SC_{12}H_{25})_4$ single crystals and carried out sc-XRD data collection on different X-ray diffractometers for no less than 10 times, we cannot obtain better results than the ones shown above. While the crystallographic data for $Sn(SC_{14}H_{29})_4$ and $Sn(SC_{16}H_{33})_4$ crystals were well collected and analyzed, there are some A and B-level alerts that cannot be removed in solving single-crystal structures of $Sn(SC_{12}H_{25})_4$. However, the simulated p-XRD of its single crystal data is highly consistent with the lab-experimental p-XRD recorded on its polycrystals (Fig. S4), indicating that sufficient and reliable atom-resolution structural information can be obtained from single crystal crystallographic data (see details in the supplementary files of crystal data and CheckCIF reports).**